Demonstration of a high-speed nonscanning imaging spectrometer

M. R. Descour, C. E. Volin, E. L. Dereniak, and K. J. Thome

Optical Sciences Center, University of Arizona, Tucson, Arizona 85721

A. B. Schumacher

U.S. Army-Tank-Automotive and Armaments Command, Warren, Michigan 48397

D. W. Wilson and P. D. Maker

Center for Space Microelectronics Technology, Jet Propulsion Laboratory, California Institute of Technology, Pasadena, California 91109

Received April 4, 1997

We report results from a field demonstration of a nonscanning high-speed imaging spectrometer [computed-tomography imaging spectrometer (CTIS)] capable of simultaneously recording spatial and spectral information about a rapidly changing scene. High-speed spectral imaging was demonstrated by collection of spectral and spatial snapshots of a missile in flight. This instrument is based on computed-tomography concepts and operates in the visible spectrum (430–710 nm). Raw image data were recorded at video frame rate (30 frames/s) and an integration time of 2 ms. An iterative reconstruction of the spatial and spectral scene information from each raw image took 10 s. We present representative missile spectral signatures from the missile firing. The accuracy of the high-speed spectrometer is demonstrated by comparison of extended-source static-scene spectra acquired by a nonimaging reference spectrometer with spectra acquired by use of CTIS imaging of the same static scenes. © 1997 Optical Society of America

Imaging spectrometry has been demonstrated to be a powerful tool in remote-sensing applications since the mid-1980's.[1] Traditional dispersive imaging spectrometers collect (x, y, λ) object-cube data by some form of scanning, such as "pushbroom" scanning (for example, the Hyperspectral Digital Imagery Collection Experiment) or "whiskbroom" scanning (for example, the Airborne Visible Infrared Imaging Spectrometer).[2,3] Alternatively, imaging Fourier-transform spectrometers equipped with a focal-plane array (FPA) at the output require scanning of the optical path difference between the two arms of a Michelson interferometer. Although these methods of data collection are acceptable for static or nearly static scenes, scanned imaging of dynamic scenes results in artifacts. In the cases of pushbroom or whiskbroom scanning imaging spectrometers, scene motion causes spatial artifacts. In the case of spectrally multiplexing spectrometers, scene motion results in spectral-signature errors. The application of computed-tomography concepts in imaging spectrometry is an effective method for overcoming these difficulties and for accomplishing instantaneous, or flash, spectral imaging. Applications that call for this form of imaging can be found in astronomy, medicine, industrial testing, and defense. The capability to acquire (x, y, λ) object-cube data at rates of 30 Hz and higher permits and enhances high-speed target recognition and location.

The connection between computed tomography and imaging spectrometry was first explored in the literature by Okamoto and co-workers[4,5] and Bulygin *et al.*[6] and later its theoretical and practical limitations were defined by Descour and Dereniak.[7] Mooney *et al.* developed a conceptually similar system for use in the infrared spectrum.[8]

The current version of the computed-tomography imaging spectrometer (CTIS) is constructed with off-the-shelf optics, with the exception of the dispersive element. The CTIS operates over the 430–710-nm bandwidth with a 10-nm spectral-sampling interval. The limitation on the CTIS bandwidth is imposed during data processing. The spectrometer consists of three optical-element groups: an objective lens, a collimator lens, and a reimaging lens. Figure 1 shows two zoom lenses and a short-focal-length lens, respectively, in these roles. The use of a zoom lens as the objective allows us to modify the field of view (FOV) of the instrument. The use of a second zoom lens as the collimator allows us to vary the magnification of the field stop onto the focal plane. Such variation can be used for adjustment of the effective dispersion within each order.[9,10] A custom computer-generated-hologram (CGH) disperser is located in collimated space between the collimator zoom lens and the reimaging lens. The FPA is a video-camera CCD array and records snapshot spectral and spatial images of the scene. All CTIS components are fixed; that is, the instrument contains no moving parts.

The CGH disperser is optimized to form a 7×7 array of diffraction orders at each wavelength within the bandpass of the CTIS. The diffraction efficiency associated with each order is inversely related to the

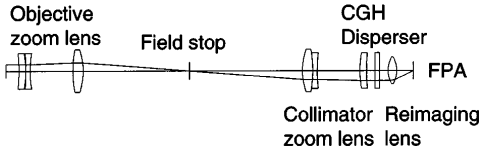

Fig. 1. Layout of the CTIS instrument.

0146-9592/97/161271-03$10.00/0

dispersion associated with that order. For example, the diffraction efficiency in the 0th-order spot is designed to be lowest, the diffraction efficiency in the highest orders is designed to be highest, and intermediate diffraction orders' efficiencies range between these two extrema. The design, fabrication, and characterization of this type of disperser have been described and executed.[11]

The effect of the imaging system is described by an $M \times N$ matrix, $\mathcal{H}$, which operates on the N-element object-cube vector, $\mathbf{f}$, and produces the M-element vector $\mathbf{g}$ representing the output image. We obtained the matrix $\mathcal{H}$ experimentally by recording the CTIS's outputs in response to a translating approximation of an (x, y, λ) point source.[7] The imaging-system model is

$$\mathbf{g} = \mathcal{H}\mathbf{f} + \mathbf{n}, \tag{1}$$

where $\mathbf{n}$ (also an M-element vector) represents additive system noise. Equations of this form often appear in image-reconstruction applications and in the case of spectrometry may be used quite generally to describe any type of instrument. The CTIS configuration reported in this Letter is configured to reconstruct an object cube measuring 18×18 spatial-resolution elements and 33 spectral samples ($N = 10,692$ voxels). The number of utilized detector elements is $M = 258,693$.

The (x, y, λ) object cube is reconstructed from raw CTIS images by means of the expectation-maximization algorithm.[12] This is an iterative algorithm that uses $\mathcal{H}$ and $\mathbf{g}$ to adjust the object-cube radiance estimate $\hat{\mathbf{f}}$.[7] The initial guess as to the object cube, $\hat{\mathbf{f}}^{(0)}$, is spatially and spectrally uniform, that is, $\hat{\mathbf{f}}^{(0)} =$ constant. We chose to stop the expectation-maximization algorithm after seven iterations. We selected this number of iterations by monitoring the least-squares agreement between the reconstructed spectra and those taken with a nonimaging reference spectrometer (Analytical Spectral Devices FieldSpec, 1° FOV) as a function of iteration number. Furthermore, we found that improved reconstruction results can be obtained if the estimated spectra are smoothed between expectation-minimization-algorithm iterations. This step suppresses the appearance of reconstruction artifacts.[13]

Figure 2 provides comparisons between field-condition spectra obtained from the CTIS and those measured simultaneously by the reference spectrometer. Spatially uniform outdoor scenes with natural or artificial content were used in the comparisons. Each scene filled the FOV and the CTIS. We judged the spatial uniformity of the scenes by comparing the fractional spatial standard deviation, $\hat{\sigma}_s = \sigma_s/\langle g \rangle$, with the fractional temporal standard deviation, $\hat{\sigma}_t = \sigma_t/\langle g \rangle$, expressed in percent. The quantity $\langle g \rangle$ is the spatial and temporal average of an ensemble of panchromatic images of each scene. The quantity $\hat{\sigma}_t$ estimates the temporal noise of the CTIS camera. In all cases, except that of coniferous vegetation, the scenes were uniform relative to the temporal noise of the instrument: blue sky, $\hat{\sigma}_s = 1.6\%$, $\hat{\sigma}_t = 2.3\%$; red brick, $\hat{\sigma}_s = 1.5\%$, $\hat{\sigma}_t = 1.6\%$; concrete pavement, $\hat{\sigma}_s = 2.3\%$, $\hat{\sigma}_t = 2.0\%$; coniferous vegetation, $\hat{\sigma}_s = 16\%$, $\hat{\sigma}_t = 1.7\%$. Spatially uniform scenes are the most difficult to reconstruct.[7]

The error bars shown in Fig. 2 are derived from the spatial variation of each reconstructed spectral signal over a 13×13 pixel region centered within the CTIS FOV. No error bars are plotted in Fig. 2(d) because the scene exhibited some lumpy structure owing to shadows, and only the mean reconstructed CTIS spectrum is shown. The accuracy of each mean CTIS spectrum was quantified through a relative spectral error (RSE), expressed in percent. Each CTIS spectrum and the corresponding reference spectrum are organized as vectors, $\hat{\mathbf{s}}$ and $\mathbf{s}_{\text{ref}}$, respectively. The RSE is defined as $\|\hat{\mathbf{s}} - \mathbf{s}_{\text{ref}}\|/\|\mathbf{s}_{\text{ref}}\|$, where $\|\mathbf{x}\|$ denotes the Euclidean norm of $\mathbf{x}$. Figure 2(a) shows a comparison of CTIS and reference-spectrometer blue-sky spectra, RSE = 3.6%; Fig. 2(b) shows a comparison of red-brick spectra, RSE = 1.4%; Fig. 2(c) shows a comparison of concrete-pavement spectra, RSE = 1.5%; and Fig. 2(d) shows a comparison of coniferous vegetation spectra, RSE = 4.4%.

A representative raw image from the missile-firing data set is shown in reversed contrast in Fig. 3. The

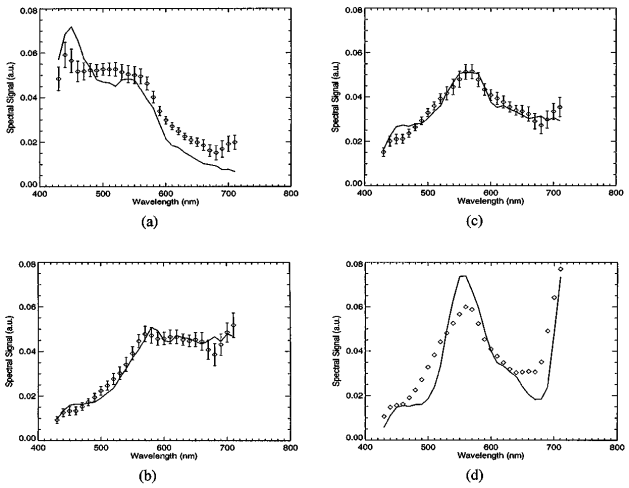

Fig. 2. Comparison of spectral signatures measured with the reference spectrometer and CTIS. ◇, CTIS spectra. See text for discussion.

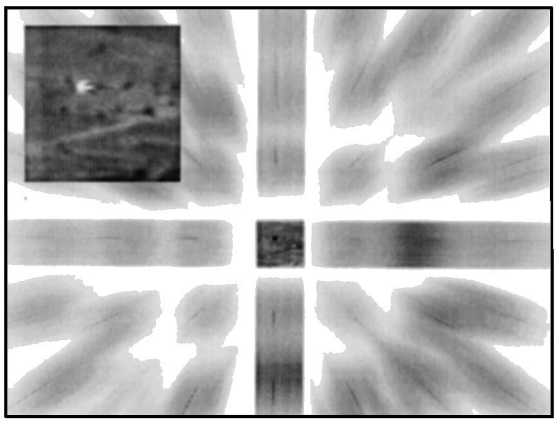

Fig. 3. Representative raw CTIS image from the missile-firing image set. The image is shown in reversed contrast. The inset shows a magnified center 0th-order image. See text for details.

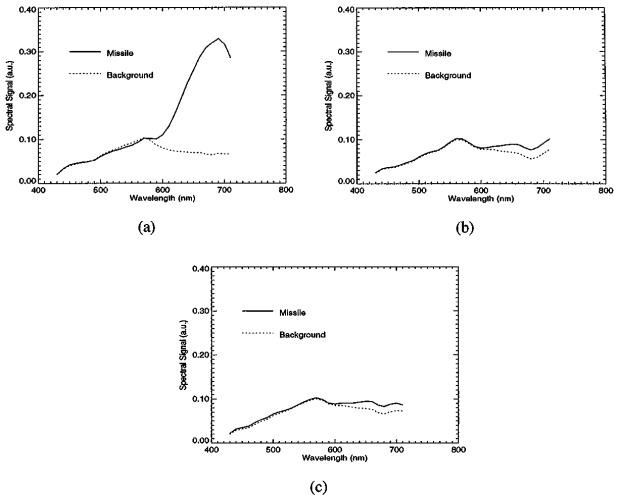

Fig. 4. Missile spectrum and corresponding background spectrum. (a)–(c) correspond to times during the missile's flight separated by 0.93 s.

entire object cube can be reconstructed from such an image. The center part of the raw image is an undispersed, panchromatic view of the scene (see Fig. 3, inset). The extent of the center image in detector elements is dictated by the field stop and the ratio of collimator-lens and reimaging-lens focal lengths (see Fig. 1). The remaining area of the FPA is dedicated to collecting dispersed replicas of the center image. Dispersion causes the blurred appearance. The center image can be used for aiming the CTIS, and no computation is required for this image to be obtained. The center image simply corresponds to the 0th diffraction order of the CGH disperser.

Each of the spectra in Fig. 4 was reconstructed from a single raw image taken at a different time during the missile's flight (Fig. 3). The dotted curves in Fig. 4 indicate background spectra taken earlier at the same instantaneous FOV that is now occupied by the missile. The solid curves in Fig. 4 represent the missile's signature at intervals of 0.93 s. The missile spectrum varies owing to increasing range and radiance fluctuations. The missile spectrum cannot be reconstructed from a single dispersed image of the scene because of the extended nonzero background that is present in the scene.

We have demonstrated a high-speed computed-tomography imaging spectrometer that contains no moving components and does not employ any form of scanning. The CTIS was used under field conditions to acquire instantaneous (x, y, λ) object-cube data on a rapidly moving missile target. The current CTIS configuration can acquire spatial and spectral data at a maximum rate of 60 fields/s with variable integration time. The frame rate ultimately depends on the readout electronics of the FPA and the minimum acceptable integration time. The minimum integration time is determined by scene radiance and desired signal level. With the current choice of camera in our system, the minimum available integration time is 100 μs. The missile's spectral signature can be used to track the missile within the CTIS FOV (see Figs. 3 and 4).

The CTIS has been shown to reproduce artificial and natural scene spectra in good agreement with spectra taken by a reference nonimaging spectrometer (Fig. 2). The scenes used in the validation of the CTIS represent the most difficult type, that is, those with little or no spatial structure.[7] The accuracy of the reconstructed spectra improves with increased scene spatial content.

Continuing research is directed in four directions: (a) enhancements of the reconstruction algorithm, such as a reduction of object-cube-reconstruction time, (b) enhancements of the CTIS components, specifically the disperser and the FPA, (c) more accurate spectral calibration, and (d) evaluation of spectral-pattern recognition techniques for high-speed target location and identification.

This work was funded in part by a California Institute of Technology President's Fund grant to M. R. Descour and D. W. Wilson.

References

1. A. F. H. Goetz, Science **228,** 1147 (1985).
2. R. W. Basedow, D. C. Carmer, and M. E. Anderson, Proc. SPIE **2480,** 258 (1995).
3. W. M. Porter and H. T. Enmark, Proc. SPIE **834,** 22 (1987).
4. T. Okamoto and I. Yamaguchi, Opt. Lett. **16,** 1277 (1991).
5. T. Okamoto, A. Takahashi, and I. Yamaguchi, Appl. Spectrosc. **47,** 1198 (1993).
6. F. V. Bulygin, G. N. Vishnyakov, G. G. Levin, and D. V. Karpukhin, Opt. Spectrosc. (USSR) **71,** 561 (1991).
7. M. R. Descour and E. L. Dereniak, Appl. Opt. **34,** 4817 (1995).
8. J. M. Mooney, V. E. Vickers, M. An, and A. K. Brodzik, "High-throughput hyperspectral infrared camera," J. Opt. Soc. Am. A (to be published).
9. M. R. Descour, "Non-scanning imaging spectrometry," Ph.D. dissertation (University of Arizona, Tucson, Ariz., 1994).
10. P. A. Bernhardt, J. Opt. Soc. Am. A **12,** 1884 (1995).
11. M. R. Descour, C. E. Volin, E. L. Dereniak, T. M. Gleason, M. F. Hopkins, D. W. Wilson, and P. D. Maker, Appl. Opt. **36,** 3694 (1997).
12. L. A. Shepp and Y. Vardi, IEEE Trans. Med. Imaging **MI-1,** 113 (1982).
13. H. E. Knutsson, P. Edholm, G. H. Granlund, and C. U. Petersson, IEEE Trans. Biomed. Eng. **BME-27,** 640 (1980).